Lactate biosensor based on a bionanocomposite composed of titanium oxide nanoparticles, photocatalytically reduced graphene, and lactate oxidase

Elena Casero[a], Concepción Alonso[b], María Dolores Petit-Domínguez[a], Luis Vázquez[c], Ana María Parra-Alfambra[a], Pablo Merino[d], Susana Álvarez-García[c], Alicia de Andrés[c], Edna Suárez[a], Félix Pariente[a], Encarnación Lorenzo[a]

[a]*Departamento de Química Analítica y Análisis Instrumental. Facultad de Ciencias. c/ Francisco Tomás y Valiente, Nº7. Campus de Excelencia de la Universidad Autónoma de Madrid. 28049 Madrid. Spain*

[b]*Departamento de Química Física Aplicada. Facultad de Ciencias. c/ Francisco Tomás y Valiente, Nº7. Campus de Excelencia de la Universidad Autónoma de Madrid. 28049 Madrid. Spain*

[c]*Instituto de Ciencia de Materiales de Madrid (CSIC). c/ Sor Juana Inés de la Cruz Nº3. Campus de Excelencia de la Universidad Autónoma de Madrid. 28049 Madrid. Spain*

[d]*Centro de Astrobiología, INTA-CSIC, Ctra. de Ajalvir km 4, 28850, Madrid, Spain*

Abstract

We have developed a lactate biosensor based on a bionanocomposite (BNC) composed of titanium dioxide nanoparticles (TiO_2-NPs), photocatalytically reduced graphene, and lactate oxidase. Graphene oxide was photochemically reduced (without using any chemical reagents) in the presence of TiO_2-NPs to give graphene nanosheets that were characterized by atomic force microscopy, Raman and X-ray photoelectron spectroscopy. The results show the nanosheets to possess few oxygen functionalities only and to be decorated with TiO_2-NPs. These nanosheets typically are at least 1 μm long and have a thickness of 4.2 nm. A BNC was obtained by mixing lactate oxidase with the nanosheets and immobilized on the surface of a glassy carbon electrode. The resulting biosensor was applied to the determination of lactate. Compared to a sensor without TiO_2-NPs, the sensor exhibits higher sensitivity (6.0 μA mM^{-1}), a better detection limit (0.6 μM), a wider linear response (2.0 μM to 0.40 mM), and better reproducibility (3.2%).

Keywords: bionanocomposite, photocatalitically reduced graphene, titanium dioxide NPs, biosensors platforms, lactate oxidase.

Introduction

Bionanocomposites based on carbon nanomaterials and metal/metal oxide nanoparticles offer a friendly platform to immobilize biomolecules due to the synergistic effect provided by their different components [1].

Among the different carbon nanomaterials, graphene, a two-dimensional lattice of sp^2-hybridized carbon, has attracted a great interest in recent years because of its unique mechanical, electrical, thermal and optical properties, opening up an exciting new research field due to its enormous potential [2-3]. In particular, a vast amount of research in this field has been focused on the development of different methods for generating graphene, each one with different advantages and disadvantages [4-6]. Among these methods, a chemical procedure, based on graphite powder oxidation in the presence of oxidants compounds and strong acids, has been widely employed because it allows to obtain graphene mass production, at low cost and with simple equipments [7-8]. This synthesis method leads to a final product, graphene oxide (GO), presenting a highly hydrophilic character due to the large number of oxygen-containing functional groups created during the oxidation process. Thus, stable suspensions of GO in water or polar organic solvents can be easily obtained by sonication. From GO, following different procedures, it is possible to diminish the oxygen-containing functional groups giving rise to reduced graphene. The most usual reduction strategy is based on the employment of chemical agents such as hydrazine or hydroquinone [9-10]. However, as a consequence of the increasing requirements towards a green chemistry, alternative methods, precluding contamination caused by the chemical reducing agents, are developed [11-12]. The as-synthesized reduced graphene is suitable for a wide number of applications ranging from electronics [13] to energy storage and conversion, i.e., supercapacitors [14], batteries [15], and fuel cells [16]. In particular, since it is a

conductive and transparent material with a high surface area, graphene has found a great applicability for electrochemical and optical biosensors development [17-19].

Nowadays, metal and metal oxide NPs have also attracted great interest as a promising interface for proteins immobilization and, therefore, for biosensor development, due to their advanced properties, such as large specific surface area, strong adsorption ability and a remarkable tendency to enhance electron-transfer between enzymes and electrodes. Although until now gold NPs and silver NPs are the most employed in fabricating biosensors [20-21], other metal and metal oxide NPs, such as palladium, platinum, ZrO_2 and ZnO ones, have also been used for this purpose [22-23]. An alternative interesting possibility is the employment of titanium dioxide NPs. This material is considered a quasi ideal narrow band gap semiconductor for photocatalysis due to its high stability, low cost and green character.

Taking into account the excellent individual properties of the as-mentioned nanostructures, their combination presents new opportunities to develop biosensors devices with improved performances. In particular, nanocomposites based on graphene and metal or metal oxides NPs have been employed to develop genosensors for the detection of sequence-specific DNA and enzymatic biosensors for glucose, cholesterol and alcohol determination [24-25]. As result of the synergistic effect of both components, the nanocomposite offers a friendly platform for enzyme or DNA immobilization and facilitates the electron transfer between the enzyme or a redox indicator and the transducer.

It is well known that development of lactate biosensors receives significant interest, due to the potential interest of this analyte as biomarker. The level of lactate in blood is an important parameter for diagnosis of patient conditions during intensive care and surgical operation process, as well as for estimating physical conditions of athletes. In

addition, in food industry the lactate level is an indicator of the fermentative process and is related to freshness, stability and storage quality of products such as tomato sauces, fruits, juices, wine and milk.

The aim of the present work is to explore the great potential of bionanocomposites based on reduced graphene, titanium dioxide NPs and lactate oxidase, deposited onto a glassy carbon surface, as environment-friendly biosensing platforms. As mentioned above, the employment of TiO_2-NPs in the development of bionanocomposites provides additional advantages for biosensor applications such as its high biocompatibility. Furthermore, since titanium dioxide is an excellent photocatalysist, it can also play a mediating role in the reduction of graphene oxide giving rise to photocatalytically reduced graphene (PRG) that is decorated with TiO_2-NPs [11, 26]. Therefore, this method offers a strategy to fabricate TiO_2/PRG nanocomposites in a single step and following a green method.

Previously to the incorporation of the enzyme, the as-synthesized TiO_2/PRG nanocomposite has been characterized by atomic force microscopy (AFM), Raman spectroscopy and X-Ray photoelectron spectroscopy (XPS) in order to determine the lateral dimensions/thickness of the sheets and to assure that the oxygen functionalities have been reduced.

As far as we know, this is the first time that photocatalytically reduced graphene and TiO_2-NPs have been employed to develop lactate oxidase based biosensors. The performance of the resulting device has been compared with that obtained for a biosensor, also developed by us [27], based on electrochemically reduced graphene and, therefore, free of titanium dioxide NPs.

Experimental Section

Materials

Ultrapure spectroscopic graphite powder (C, particle size 50.0–50.3 μm) was obtained from United Carbon Products Co. Inc. (Bay City, MI, USA). Lactate oxidase (LOx, EC 232-841-6 from Pediococcus species) lyophilized powder containing 41 units/mg solid was obtained from the Sigma Chemical Co. (St. Louis, MO, http://www.sigmaaldrich.com). Stock solution was prepared dissolving 1.3 mg of the LOx lyophilized powder in 250 μL of 0.1M phosphate buffer solution (pH=7.0), aliquoted (10 μL) and stored at -30ºC. Under these conditions the enzymatic activity remains stable for several weeks. L-(+)-lactic acid lithium salt 97%, hydroxymethylferrocene (HMF), N,N'-Dimethylformamide, potassium persulfate, phosphorus pentoxide, potassium permanganate and hydrogen peroxide were obtained from Aldrich Chemical Co. (Milwaukee, WI, http://www.sigmaaldrich.com). Titanium (IV) isopropoxide ($C_{12}H_{28}O_4Ti$) was also purchase from Aldrich Chemical Co (Product Number: 377996, CAS-No.: 546-68-9). Other chemicals used in this work, such as sulphuric acid, ethanol (99.5% v/v), hydrochloric acid and sodium phosphate were reagent grade quality and used as received without additional purification steps. Sodium phosphate (http://www.merck.com) was employed for the preparation of buffer solutions. Water was purified with a Millipore Milli-Q-System (http://www.millipore.com). All solutions were prepared just prior to use.

Experimental techniques

The phases present in the coating were determined by using a X-ray diffractometry (X'Pert PRO XRD, Panalytical) at a glancing angle of 0.5º using a Cu K_α line generated at 40 mA, 45 kV: start position [°2theta] 5.0100; end position [°2theta] 39.9900; step

size [°2theta] 0.0167; scan step time [s] 100 with x´celerator detector. The diffractometer works with the wavelength of copper, which is 1.5406 nm.

The AFM measurements were performed in air with Nanoscope IIIa (Veeco) and Agilent 5500 (Agilent) equipments. The images were taken in the dynamic mode using silicon cantilevers (Bruker) with a nominal force constant of 40 N/m. First, large areas (around 100 μm^2) were scanned in order to locate the graphene structures which were then imaged at higher resolution. The images, 512 x 512 pixels, were taken with different cantilevers in order to ensure that the imaged structures were not due to tip artefacts. Supports used in AFM and XPS measurements were Si substrates from University Wafer, USA. Note that on the Si surface there is a very thin layer of native SiO_2 (1-2 nm) formed after air exposure. Thus, we denote these substrates as Si/SiO_2.

Micro-Raman experiments were performed at room temperature with the 488 nm line of an Ar^+ laser with incident power in the range 0.1–1 mW. The light is focused and collected with an Olympus microscope (x100 objective) and a “super-notch-plus” filter from Kaiser is used to eliminate the elastic light. The scattered light is analyzed with a Jobin -Yvon 460HR monochromator coupled to liquid nitrogen cooled CCD.

The XPS experimental set up consists in an ultra high vacuum chamber with a base pressure of 10^{-10} mbar. The chamber is equipped with a Phoibos 150 hemispherical energy analyzer and an X-Ray source XR50 both from SPECS. The XPS spectra analysis was done using the FITT program after a Shirley background subtraction, the default lorentzian width is 0.3 eV and the default gaussian width is 1.6 eV. The sample energy was calibrated using the Si2p core level peak which appears at 99 eV, using this reference we find shifts of -0.19 eV and -0.79 eV for GO and TiO_2/PRG, respectively.

UV-irradiation of TiO_2-GO mixtures was performed using an Oriel 450 W xenon arc lamp in order to obtain photocatalytically reduced graphene.

Cyclic voltammetric studies were carried out with an Ecochemie Autolab PGSTAT12 system (Utrecht, The Netherlands, http://www.ecochemie.nl). The electrochemical experiments were carried out in a three-compartment cell with a working glassy carbon electrode and a platinum wire as counter electrode (http://www.metrohm.com). All potentials were reported with respect to a Ag/AgCl reference electrode without taking into account the liquid junction. All solutions were deaerated with nitrogen gas before use, keeping the gas flow over the solutions during experiments.

Procedures

Synthesis of graphene oxide

Graphene oxide was synthesized from graphite powder by a modified Hummers method [7]. The solid obtained was dried in air and mixed with 5 mM phosphate buffer solution (pH=7.0), obtaining a 0.5 mg mL^{-1} graphite oxide dispersion. Exfoliation was carried out by sonicating it during one hour. The resulting product, denoted as graphene oxide, was subsequently reduced following photocatalytical procedures [11].

Synthesis of TiO_2 colloidal suspension

The preparation of the TiO_2 colloids in the nanometer range can be performed through the hydrolysis and condensation of titanium alkoxides. In order to prepare a TiO_2 colloidal suspension, 20 µL of titanium isopropoxide was added to a vigorously stirred solution of 10 mL of ethanol (99.5% v/v) at room temperature [11]. Since there is a 0.5% of water, the $[H_2O]$ / $[C_{12}H_{28}O_4Ti]$ molar ratio was of 28 and the pH was 8.6. Stirring is mandatory in order to prevent agglomeration of the particles. The resulting colloidal suspension was subsequently employed for the UV-induced photocatalytic reduction of graphene oxide.

187 **Synthesis of photocatalytically reduced graphene**

188 UV-induced photocatalytic reduction was carried out from the as-synthesized GO and
189 TiO_2 colloidal suspension, following a published procedure [11]. The resulting product,
190 denoted as photocatalytically reduced graphene, was redispersed in EtOH, leading to a
191 final concentration of 0.5 mg mL^{-1}.

192 **Preparation of the samples used for XRD, AFM, Raman and XPS measurements**

193 TiO_2 samples for XRD and AFM measurements were prepared by deposition of 100
194 μL and 10 μL of TiO_2 stirred colloidal suspension in ethanol on Si/SiO_2 surfaces,
195 respectively and allowing them to air-dry.

196 GO and/or TiO_2/PRG samples for AFM, Raman and XPS measurements were
197 prepared by deposition of 10 μL of the corresponding stock dispersion on Si/SiO_2
198 surfaces and allowing them to air-dry.

199 **Preparation of the electrochemical biosensing platforms**

200 Prior to each experiment, glassy carbon (GC) electrodes were polished with 1 μm
201 diamond paste (Buehler) and rinsed with water. The TiO_2/PRG/GC modified electrodes
202 were prepared by placing 10 μL of the TiO_2/PRG stock suspension on the GC electrode
203 surface. After air-dried, the modified electrodes were washed with ethanol. The
204 electrochemical biosensing platform, denoted as LOx/TiO_2/PRG/GC, was developed by
205 placing 10 μL of the LOx stock solution onto the TiO_2/PRG/GC electrode surface. After
206 air-dried, the modified electrodes were washed with water to remove any weakly bound
207 material.

208

209 **Results and discussion**

210 We have synthesized photocatalytically reduced graphene by subjecting a mixture
211 of graphene oxide and a TiO_2 colloidal suspension to UV irradiation. Therefore, in a

first step we have obtained a titanium dioxide NPs following the procedure described in the experimental section and subsequently we have characterized them by XRD and AFM. Figure S1A shows the X-ray diffraction pattern of the as-synthesized TiO_2-NPs deposited onto a Si/SiO_2 surface. The observed diffraction peaks, centered at $2\theta=25°$, 38°, 48°, 55° and 63°, correspond to (110), (200), (112), (220) and (310) planes, which indicates the formation of single phase titanium dioxide [28].

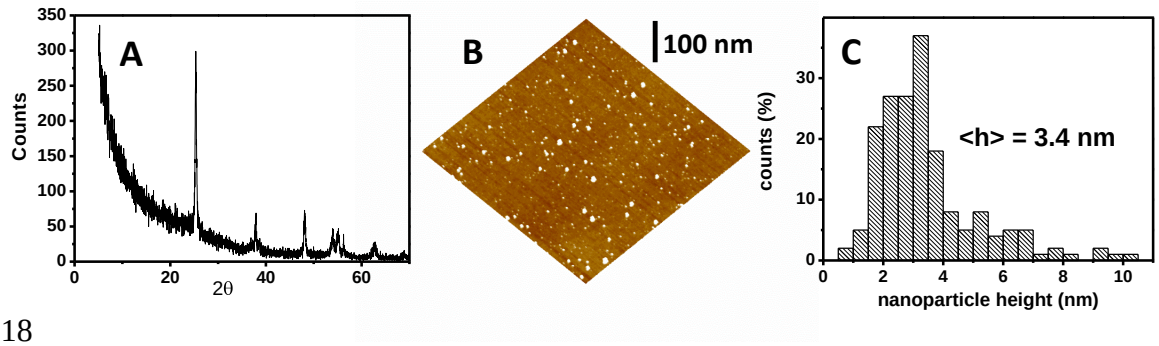

Figure S1. (A) XRD pattern, (B) AFM image of TiO_2-NPs deposited onto a Si/SiO_2 substrate, (C) Height distribution corresponding to the image in figure S1B.

In addition, atomic force microscopy technique was employed to study the morphological characteristics of the same sample. Figure S1B shows a 2.5 μm x 2.5 μm AFM image of TiO_2-NPs deposited onto a Si/SiO_2 surface. Isolated nanoparticles are imaged displaying different sizes. As the measured diameter is affected by tip convolution effects, in order to obtain the size distribution of the nanoparticles, we have measured their height. Thus, we have measured up to 300 nanoparticles to have enough statistics and the corresponding height histogram is shown in figure S1C. From this distribution, we obtain an average size of 3.4 nm ± 1.7 nm.

In a second step, graphite oxide was prepared following the modified Hummers method described in the experimental section, which involves oxidation of graphite powder by addition of strong acids and oxidant agents. Since the degree of oxidation

232 deeply depends on both the reaction conditions and the graphite precursor employed, an
233 exhaustive characterization of the synthesized nanomaterial has been performed by
234 several techniques. In order to do this, the resulting graphite oxide obtained by the
235 modified Hummers method is exfoliated by sonication in an aqueous media to produce
236 stable dispersions of thin graphene oxide sheets. These GO sheets have been
237 characterized by X-Ray diffraction spectroscopy (XRD), X-Ray photoelectron
238 spectroscopy (XPS) and atomic force microscopy (AFM). The information gathered by
239 this combination of techniques can be summarized as follows: i) from XRD, it can be
240 concluded that the synthesis of GO is successfully achieved because the spectra displays
241 a diffraction peak centered at $2\theta=10.4^{o}$, which is typical of GO; ii) AFM allows to
242 conclude that the synthesis methodology affords the production of GO nanosheets that
243 present a typical lateral dimension of several hundreds of nanometers and a thickness
244 value of 1.3 ± 0.1 nm; iii) XPS data shows that the synthesized GO contains sp^2-
245 hybridized carbon and at least four types of carbon bonded to different oxygen
246 functional groups (C-OH, C-O, C=O and O-C=O), indicating a considerable oxidation
247 degree [27].

248 From the as-synthesized GO, we have prepared reduced graphene. The reduction
249 step, which can be achieved by different methods, a diminution of the oxygenated
250 functionalities. In our case, we have employed a photocatalytic method based on
251 irradiating a mixture of GO and TiO_2-NPs with UV-light [11]. As GO accepts electrons
252 from UV irradiated TiO_2 suspensions, a change in color of the suspensions from brown
253 to black takes place, as can be observed in figure S2 (A, B, C). TiO_2 is a semiconductor
254 whose band gap corresponds to light of approximately 350 nm. Irradiation at this
255 wavelength promotes electrons from the valence band of the material to the conduction
256 band, generating electron-hole pairs (figure S2D, reaction 1). Most of these pairs (90%)

recombine within picoseconds, but some persist for at least a few nanoseconds [29]. These surviving electron-hole pairs can produce various reactive species, depending upon the environment in which they are created. In a N_2-saturated ethanolic environment, the holes are scavenged to produce ethoxy radicals (figure S2D, reaction 2), leading to an electron accumulation in TiO_2-NPs.

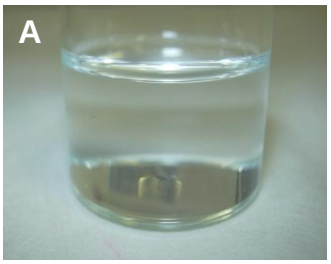

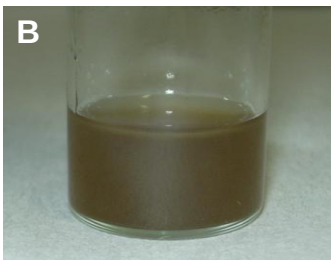

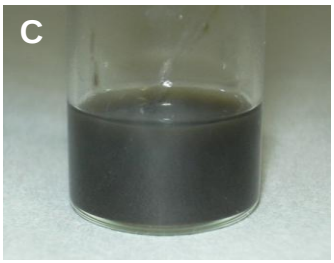

D

$$TiO_2 + h\nu \ (350\ nm) \rightarrow TiO_2\,(holes / electrons) \quad (1)$$

$$TiO_2\,(holes / electrons) \xrightarrow{C_2H_5OH} TiO_2(electrons) + C_2H_5O^* + H^+ \quad (2)$$

$$TiO_2\,(electrons) + GO \longrightarrow TiO_2 + PRG \quad (3)$$

Figure S2. 10 mM TiO_2 colloidal suspension in ethanol (A), mixture of GO and TiO_2 colloidal suspension before (B) and after (C) 3 hours of UV irradiation. (D) Mechanism of the TiO_2-UV-assisted photocatalytic reduction of graphene oxide.

In presence of electron acceptors, such as fullerenes and carbon nanotubes, decreases the trapped electrons in the TiO_2 particles [30]. In the same way, the excited TiO_2–NPs reduce the oxygenated functionalities of GO, such as carboxylic acid, epoxy and hydroxyl groups, allowing to obtain reduced graphene (figure S2D, reaction 3).

A typical image of the resulting composite material (TiO_2/PRG) is shown in figure 1A. A sort of platelet is imaged that resembles those found for electrochemically reduced graphene [27], but clearly rougher and higher. This increase in roughness and

height is related to the relative large amount of rounded nanostructures imaged at the surface that we associate to the presence of titanium dioxide NPs. Thus, from these data, we consider that the platelet is composed by the PRG sheet and TiO_2 nanoparticles.

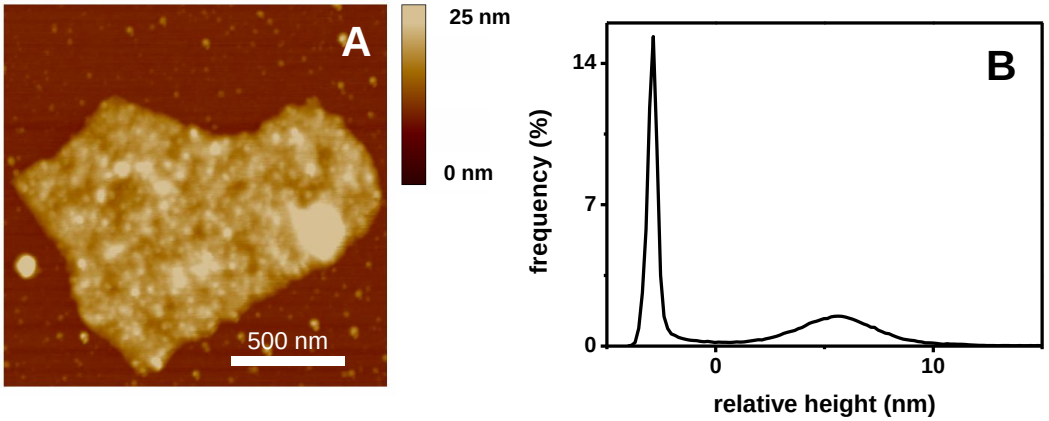

Figure 1. (A) 1.6 x 1.6 μm^2 AFM image of a photocatalytically reduced graphene sheet with TiO_2 nanoparticles on Si/SiO_2 substrate obtained in dynamic mode at air. (B) Height distribution corresponding to the image in figure 1A. The height difference between the two maxima corresponds to the average thickness of the platelet structure.

It is worth to note that these nanoparticles are also found scattered on the surrounding Si/SiO_2 substrate area.

As it is mentioned above, the figure clearly shows that there are TiO_2-NPs on top of the platelet structure, which leads to a relatively rough morphology. Moreover, it is very likely that, due to the sample preparation, below this structure there are also some TiO_2 nanoparticles since they could become attached to both sides of the graphene sheet. This fact, which can further contribute to the observed uneven morphology of the platelet surface, clearly hampers the estimation of the PRG sheet thickness. Thus, the average height of the platelet, which includes both the graphene and TiO_2-NPs, can be estimated from the height distribution of the image (figure 1B). In this distribution two maxima

are clearly observed, the narrowest one corresponding to the bare silicon surface and the broadest to the platelet structure. These maxima are separated (x-axis) by 8.5 nm, which is then the average thickness of the rough platelet. In order to have an estimation of PRG sheet thickness, we can consider the height of the lowest site on the platelet, which is 4.2 nm. However, this value is likely an overestimation of the PRG sheet thickness since the presence of TiO_2-NPs between the silicon substrate and the bottom side of the PRG sheet cannot be discarded but rather is very likely.

In order to further evaluate the quality of the as- synthesized TiO_2/PRG, we have employed Raman spectroscopy that is a powerful technique to characterize carbonaceous materials. The Raman spectra of GO and TiO_2/PRG are compared in figure 2. In GO, the band around 1350 cm^{-1}, denoted as D, is related to the presence of a high concentration of defects but, since it is associated to a breathing mode of the sp^2-C rings, its intensity increases during the first steps of the reduction processes. The elimination of functional groups during the reduction increases the density of rings and therefore the intensity of the D band increases, as observed in figure 2 where the I_G/I_D ratio increases from 0.8 to 1.03. The decrease of D and G band widths (in the present case around 25%) is also an evidence of the elimination of defects. The photochemical process is therefore able to eliminate a significant fraction of the functional groups.

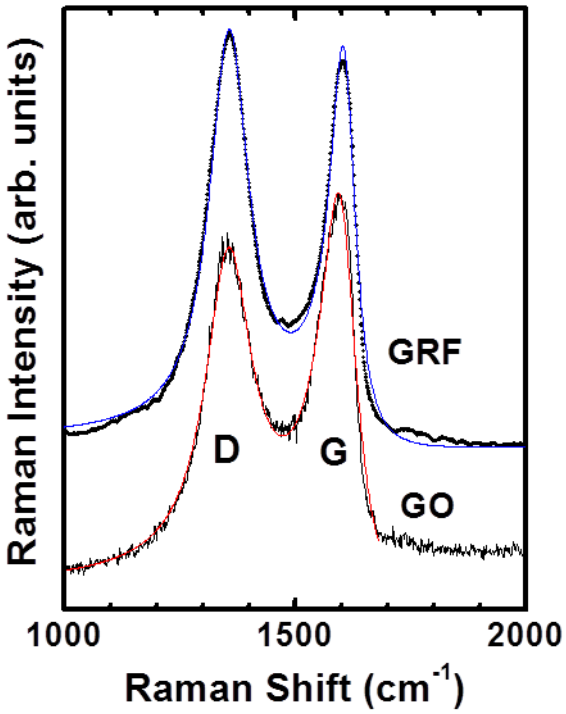

Figure 2. Raman spectra of GO and TiO_2/PRG samples. Red and blue lines are the fits of the experimental data for GO and TiO_2/PRG respectively. Excitation at 488 nm.

In order to determine the fraction of the functional groups eliminated during the reduction process, we have performed X-Ray photoelectron spectroscopy (XPS) measurements. This technique is very helpful to determine the chemical composition of substances, since the XPS core level peak of a given element can be decomposed in different components, each one can be attributed to a particular chemical state. The XPS spectra (C1s) of GO and TiO_2/PRG are presented in figure 3A and 3B, respectively. The C1s core level of GO results in a highly asymmetric peak and several curves are needed for a good fit (figure 3A). Following previous works, its decomposition can be

performed in terms of C-C sp^2 (284.8 eV), C-OH (285.7 eV), C-O (286.6 eV), C=O (287.5 eV) and O-C=O (289.0 eV) components [27, 31, 32]. The ratio between the largest component, corresponding to the signal coming from carbon atoms in the sp^2 configuration, and the other four components, corresponding to signals coming from carbon bonded to different oxygen functionalities (C-OH, C-O, C=O and O-C=O), is 0.73, indicating a considerable oxidation degree. After the reduction process (figure 3B), this ratio reaches a value of 2.05. Thus, the amount that can be attributed to carbon in the sp^2 configuration rises from an original 42.3% in GO to 67.2% in TiO_2/PRG. Moreover, from a visual comparison between figure 3A and 3B, it is clear that after the reduction process, an increase of the peak intensity of the component corresponding to C-C sp^2 concomitant with a decrease of the peak intensities of the components corresponding to carbon bonded to oxygen functionalities has been occurred. In particular, the C=O, C-OH, C=O and O-C=O components diminish by 9.4%, 8.9%, 5.8% and 0.8%, respectively, which represents a global diminution of 25% in the peak intensities of the oxygen-related components. Note that although the C=O and O-C=O components diminish their relative area, they become less modified than the C=O, C-OH components. Thus, from these data it can be concluded that photoreduction is an efficient process able to diminish the oxidation degree of a GO sample up to 25% and particularly effective for C=O and C-OH species.

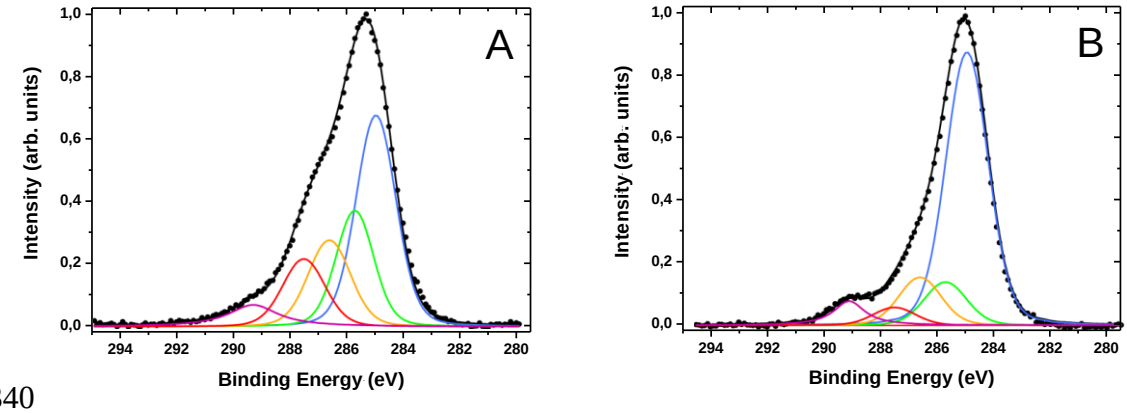

Figure 3. C1s XPS spectra of (A) graphene oxide (GO) and (B) photocatalytically reduced graphene (TiO_2/PRG). The decomposition in curve components is shown in color scale underneath the data points. The black line corresponds to the sum of all the individual components.

The reduction process can also be corroborated from the O1s peak (data not shown). For TiO_2/PRG, the energy of this peak appears at 532.5 eV, which is the energy value of the oxygen peak in Si/SiO_2 used as substrate. When GO is measured on a Si/SiO_2 substrate, the value shifts to 533.0 eV due to the sum of both contributions (oxygen functionalities coming from GO and from SiO_2). Finally, it is important to note that there also appears a component with an energy value of 530.6 eV, corresponding to oxygen bonded to Ti (in a TiO_2 stoichiometry) and a peak around 460 eV corresponding to Ti2p. Both peaks confirm the presence of TiO_2 in the nanocomposite (data not shown).

In a previous work [27], we have reported the synthesis, characterization and applicability of graphene oxide and electrochemically reduced graphene in the development of lactate biosensing platforms, as case of study. In order to continue with this line of research, we have also employed the as-synthesized nanocomposite (TiO_2/PRG) to fabricate a biosensor for lactate determination, as described in the experimental section. The resulting LOx/TiO_2/PRG/GC biosensor, in presence of oxygen, catalyzes the oxidation of lactate into pyruvate and hydrogen peroxide. Thus, the activity of the immobilized LOx can be electrochemically detected by monitoring the H_2O_2 produced in the enzymatic reaction. The resulting cyclic voltammetric response (data not shown) exhibits an irreversible anodic wave at high overpotential. However, the measurement of the direct oxidation of the hydrogen peroxide generated in the enzymatic reaction does not represent an adequate strategy to determine lactate

because it can be affected by potential interfering species present in the sample, which could also be oxidized at the high potential required for H_2O_2 amperometric detection. In order to minimize the contribution of interfering substances to the lactate biosensor response, one of the most important approaches reported in the literature is based on the replacement of the natural electron acceptor (O_2) by an artificial mediator. Based on our previous experience with other oxidases, we have selected the hydroxymethylferrocene (HMF) to act as a redox mediator in solution. In this case, LOx catalyzes the oxidation of lactate to pyruvate, while the electrons involved in the process are immediately transferred to the oxidized form of the soluble redox mediator (HMF), regenerating the enzyme activity. The re-oxidation of HMF on the electrode surface leads to a catalytic response of the biosensor proportional to the amount of substrate, lactate, present in the solution.

Figure 4A displays the cyclic voltammetric response for LOx/GC in contact with a 0.1 M pH=7.0 phosphate buffer containing 1.0 mM HMF in the absence (a) and in the presence (b) of lactic acid.

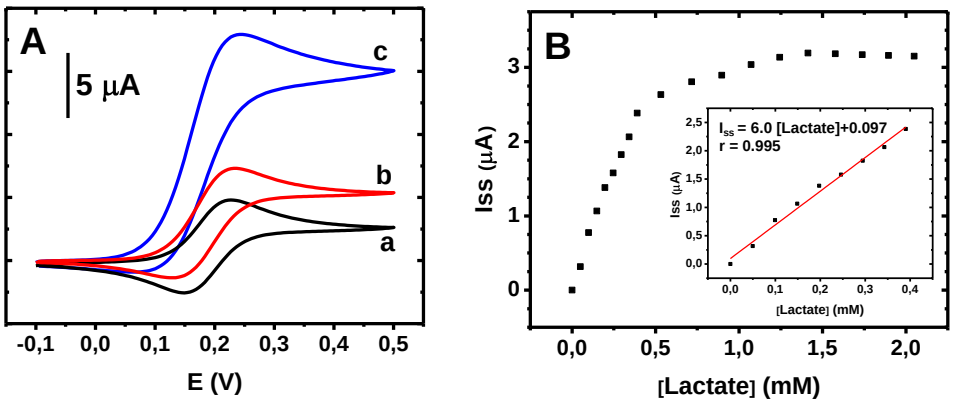

Figure 4. (A) Cyclic voltammetric response in 0.1 M phosphate buffer pH=7 containing 1.0 mM HMF for: a) LOx/GC in the absence of lactate, b) LOx/GC in the presence of 3 mM of lactate and c) LOx/TiO_2/PRG/GC in the presence of 3 mM of lactate. Scan rate 0.01 V/s. (B) Calibration curve obtained from chronoamperometric measurements (E=+0.25 V) for LOx/TiO_2/PRG/GC biosensor in phosphate buffer 0.1 M pH=7

containing 1.0 mM HMF in presence of increasing amounts of lactate. Inset: Linear part of 4B and the corresponding fit to a linear regression equation.

As can be seen, in scan a, the typical redox response of the ferrocene/ferrocinium process in aqueous media is observed. Upon addition of lactic acid to a final concentration of 3 mM, there is an enhancement of the anodic peak current concomitant with a decrease of the cathodic peak current, which is consistent with an electrocatalytic effect (scan b). The cyclic voltammetric response for LOx/TiO_2/PRG/GC, in the same experimental conditions, is displayed in scan c. From comparison between the catalytic currents obtained with (scan c) and without (scan b) TiO_2/PRG, it is evident that the employment of the nanomaterial in the biosensor construction enhances significantly the analytical response of the resulting device. Chronoamperometric measurements of LOx/TiO_2/PRG/GC platforms for different lactate concentrations were carried out by posing the biosensor at a constant potential of +0.25 V (starting at -0.05 V, where no redox process occurs). The current measured at this time was plotted as a function of the concentration of lactate in solution (figure 4B). These experimental data were fitted to a Michaelis-Menten equation by means of non-linear regression, obtaining a K'_M value of 0.32 mM. This value indicates the grade of affinity of the immobilized enzyme to the substrate and it is correlated to the linear range biosensor response. The K'_M value obtained is comparable to other ones reported in the literature for LOx based biosensors, in which the enzyme is covalently bound to modified gold electrodes [33]. The analytical properties of the developed biosensor, such as sensitivity, linear concentration range, detection limit and reproducibility were evaluated (table 1). As can be seen in this table, the biosensor can measure lactate from 2.0×10^{-3} mM to 0.40 mM and its sensitivity, calculated as the slope of the calibration curve, was 6.0 $\mu A\ mM^{-1}$. Concerning the detection limit, calculated as the ratio between three times the standard

deviation of the blank signal and the sensitivity, a value of 0.60 x 10^{-3} mM was obtained. Finally, the reproducibility was evaluated from the RSD for five different measurements of 0.25 mM of lactate with the same biosensor, yielding around 3.2%. In order to compare the analytical properties obtained for the developed biosensor with those of other lactate biosensors, we have also included in table 1 data concerning linear concentration range, sensitivity, detection limit and reproducibility of several lactate-based biosensors reported in the literature [21, 22, 23, 27, 34, 35]. It is important to highlight that most of the biosensors summarized in the table include nanomaterials, such as metal nanoparticles, carbon nanotubes and graphene or they employed nanostructured transducers such as rough gold surfaces and 3-dimensional ordered macroporous (3DOM) gold electrodes. Due to the different nature of biosensors displayed in table 1, a high variability of data is observed for each analytical parameter. However, it can be concluded that most of the analytical properties of the biosensor designed by us are comparable or even better than those reported in the literature for other lactate-based biosensors.

Table 1. Analytical properties of several lactate based biosensors reported in the literature including the present work.

Lactate sensors	**Linear range (mM)**	**Sensitivity (μA mM^{-1})**	**Detection limit (μM)**	**R.S.D. (%)**
LOx/TiO_2/PRG/GC (Present work)	$2.0x10^{-3}$ – 0.40	6.0	0.60	3.2 (C=0.25 mM, n=5)
LOx/ERG/GC [27]	0.025 - 0.25	3.2	7.5	6.1 (C=0.20 mM, n=5)
LOx/Au [35]	Up to 0.3	0.77±0.08	10	8 (C=0.15 mM, n=3)
LOx/DTSP/Au [35]	Up to 0.2	0.69±0.08	40	8 (C=0.15 mM, n=3)
LOx /AuNPs /MPTS/Au [21]	0.05–0.25	3.4	4.0	5
LOx/MWCNT/PtNPs/TEOS/GC [22]	0.25–2.0	6.36	0.3	-
LOx/CoPh/MnO_2NPs/chitosan/GC [34]	0.020–4.0	3.98	8	4.6
LOx/Au_R [33]	Up to 1.3	----	29.8	4.2 (C=0.5 mM, n=5)
LOx/DTSP/Au_R [33]	Up to 1.2	----	21.5	3.9 (C=0.5 mM, n=5)
LOx/Au_{3DOM} [33]	Up to 0.6	----	16.2	3.9 (C=0.5 mM, n=5)
LOx/DTSP/Au_{3DOM} [33]	Up to 1.3	----	3.9	3.5 (C=0.5 mM, n=5)
PDDA/LOx/ZnO/MWCNT/PG [23]	0.2-2.0	7.3	6	-

LOx=lactate-oxidase, TiO_2=Titanium dioxide nanoparticles, PRG=photocatalytically reduced graphene, GC=glassy carbon electrode, Au= gold electrode, DTSP=3,3´-dithiodipropionic acid di(N-succinimidyl ester, AuNPs= gold nanoparticles, MPTS= (3-mercaptopropyl)-trimethoxysilane, MWCNTs=multiwalled carbon nanotubes, PtNPs: platinum nanoparticles, CoPh=cobalt phthalocyanine colloid, MnO_2NPs=Manganese dioxide nanoparticles, LDH=lactate dehydrogenase, Au_R=rough gold electrode, Au_{3DOM}=three-dimensional ordered macroporous gold electrode, PDDA= polydiallyldimethylammonium chloride, ZnO=zinc oxide nanoparticles, , PG= pyrolytic graphite, PET=polyester

In particular, when we compare the analytical properties of the lactate biosensor based on TiO_2/PRG nanocomposite with those of a similar biosensor developed by us, but including graphene that has been reduced following electrochemical procedures, TiO_2/PRG/GC shows a higher sensitivity and reproducibility, as well as a lower detection limit [27].

4. Conclusions

TiO_2/PRG nanocomposite has been fabricated by a green method consisting in UV-assisted reduction of graphene oxide, previously synthesized employing a modified Hummers method, in the presence of TiO_2-NPs. The employment of AFM, Raman and XPS techniques allows to confirm that the resulting material is formed by graphene nanosheets (around 1 μm of lateral dimension and a thickness smaller or equal than 4.2 nm), with a low amount of oxygen functionalities and decorated with TiO_2 nanoparticles.

This nanocomposite, in conjunction with LOx, leads to a bionanocomposite that deposited onto a glassy carbon electrode was employed as a lactate biosensing platform. This integrated LOx/TiO_2/PRG/GC system, photocatalytically generated, exhibits a higher electrocatalytic activity for lactate determination with a wider linear range and a lower LOD, when compared with an electrochemically reduced graphene based lactate biosensor.

Acknowledgments

This work has been supported by Comunidad Autónoma de Madrid (project No. S2009/PPQ-1642, AVANSENS), Ministerio de Ciencia e Innovación (project No. CTQ2011-28157) and Ministerio de Economía y Competitividad (project No. FIS2012-38866-C05-05). We want to give thanks to Noemí González Díaz and Mario Ramírez Fernández from XRD polycrystalline laboratory of SIdI (UAM). P.M. thanks INTA for a "Rafael Calvo Rodés" FPI scholarship.

468 **REFERENCES**

469 **1.** Lu W, Luo Y, Chang G, Sun X (2011) Synthesis of functional SiO_2-coated
470 graphene oxide nanosheets decorated with Ag nanoparticles for H_2O_2 and
471 glucose detection. Biosens Bioelectron 26:4791-4797

472 **2.** Guo S, Dong S (2011) Graphene nanosheet: synthesis, molecular engineering,
473 thin film, hybrids, and energy and analytical applications. Chem Soc Rev
474 40:2644-2672

475 **3.** Pumera M, Ambrosi A, Bonanni A, Chng ELK, Poh HL (2010) Graphene for
476 electrochemical sensing and biosensing. TrAC-Trend Anal Chem 29:954-965

477 **4.** Kosynkin DV, Higginbotham AL, Sinitskii A, Lomeda JR, Dimiev A, Price
478 K, Tour JM (2009) Longitudinal unzipping of carbon nanotubes to form
479 graphene nanoribbons. Nature 458:872-876

480 **5.** Jiao L, Zhang L, Wang X, Diankov G, Dai H (2009) Narrow graphene
481 nanoribbons from carbon nanotubes. Nature 458:877-880

482 **6.** Elías AL, Botello-Méndez AR, Meneses-Rodríguez D, González VJ,
483 Ramírez-González D, Ci L, Muñoz-Sandoval E, Ajayan PM, Terrones H,
484 Terrones M (2010) Longitudinal cutting of pure and doped carbon nanotubes to
485 form graphitic nanoribbons using metal clusters as nanoscalpels. Nano Lett
486 10:366-372

487 **7.** Hummers WS, Offeman RE (1958) Preparation of graphitic oxide. J Am
488 Chem Soc 80:1339-1339

489 **8.** Park S, Ruoff RS (2009) Chemical methods for the production of graphenes.
490 Nat Nanotechnol 4:217-224

491 **9.** Stankovich S, Dikin DA, Piner RD, Kohlhaas KA, Kleinhammes A, Jia YY,

492 Wu Y, Nguyen ST, Ruoff RS (2007) Synthesis of graphene-based nanosheets
493 via chemical reduction of exfoliated graphite oxide. Carbon 45:1558-1565

494 **10.** Wang GX, Yang J, Park J, Gou XL, Wang B, Liu H, Yao J (2008) Facile
495 synthesis and characterization of graphene nanosheets. J Phys Chem C
496 112:8192-8195

497 **11.** Williams G, Seger B, Kamat PV (2008) TiO_2-graphene nanocomposites.
498 UV-assisted photocatalytic reduction of graphene oxide. ACS Nano 2:1487-
499 1491

500 **12.** Guo H-L, Wang X-F, Qian Q-Y, Wang F-B, Xia X-H (2009) A green
501 approach to the synthesis of graphene nanosheets. ACS Nano 3:2653-2659

502 **13.** Hass J, de Heer WA, Conrad EH (2008) The growth and morphology of
503 epitaxial multilayer graphene. J Phys-Condens Mat 20:323202(1-27)

504 **14.** Stoller MD, Park SJ, Zhu YW, An JH, Ruoff RS (2008) Graphene-based
505 ultracapacitors. Nano Lett 8:3498-3502

506 **15.** Yoo E, Kim J, Hosono E, Zhou H, Kudo T, Honma I (2008) Large reversible
507 Li storage of graphene nanosheet families for use in rechargeable lithium ion
508 batteries. Nano Lett 8:2277-2282

509 **16.** Shang N, Papakonstantinou P, Wang P, Silva SRP (2010) Platinum
510 integrated graphene for methanol fuel cells. J Phys Chem C 114:15837-15841

511 **17.** Gan T, Hu S (2011) Electrochemical sensors based on graphene materials.
512 Microchim Acta 175:1-19

513 **18.** Kuila T, Bose S, Khanra P, Mishra AK, Kim NH, Lee JH (2011) Recent
514 advances in graphene-based biosensors. Biosens Bioelectron 26:4637-4648

19. Pumera M (2011) Graphene in biosensing. Mater Today 14:308-315

20. Pingarrón JM, Yáñez-Sedeño P, González-Cortés A (2008) Gold nanoparticle-based electrochemical biosensors. Electrochim Acta 53:5848-5866

21. Parra-Alfambra AM, Casero E, Petit-Domínguez MD, Barbadillo M, Pariente F, Vázquez L, Lorenzo E (2011) New nanostructured electrochemical biosensors based on three-dimensional (3-mercaptopropyl)-trimethoxysilane network. Analyst 136:340–347

22. Huang J, Li J, Yang Y, Wang X, Wu B, Anzai J, Osa T, Chen Q (2008) Development of an amperometric l-lactate biosensor based on l-lactate oxidase immobilized through silica sol–gel film on multi-walled carbon nanotubes/platinum nanoparticle modified glassy carbon electrode. Mater Sci Eng C, 28:1070–1075.

23. Wang YT, Yu L, Wang J, Lou L, Du WJ, Zhu ZQ, Peng H, Zhu JZ (2011) A novel l-lactate sensor based on enzyme electrode modified with ZnO nanoparticles and multiwall carbon nanotubes. J Electroanal Chem 661:8-12

24. Jang HD, Kim SK, Chang H, Roh KM, Choi JW, Huang J (2012) A glucose biosensor based on TiO_2–Graphene composite. Biosens Bioelectron 38:184-188

25. Saini D, Chauhan R, Solanki PR, Basu T (2012) Gold-nanoparticle decorated graphene-nanostructured polyaniline nanocomposite-based bienzymatic platform cholesterol sensing. International Scholarly Research Network, ISRN Nanotechnology 2012:ID 102543(1-12)

26. Zou F, Yu Y, Cao N, Wu L, Zhi J (2011) A novel approach for synthesis of TiO_2–graphene nanocomposites and their photoelectrical properties. Scripta Mater 64:621-624

27. Casero E, Alonso C, Vázquez L, Petit-Domínguez MD, Parra-Alfambra AM, de la Fuente M, Merino P, Álvarez-García S, de Andrés A, Pariente F, Lorenzo E (2013) Comparative response of biosensing platforms based on synthesized graphene oxide and electrochemically reduced graphene. Electroanal 25:154-165

28. PDF database by the Joint Committee for Powder Diffraction Standards (JCPDS)

29. Serpone N, Lawless D, Khairutdinov R, Pelizzetti E (1995) Subnanosecond relaxation dynamics in TiO_2 colloidal sols (particle sizes Rp = 1.0-13.4 nm). Relevance to heterogeneous photocatalysis. J Phys Chem 99:16655-16661

30. Kamat PV, Bedja I, Hotchandani S (1994) Photoinduced charge transfer between carbon and semiconductor clusters. One-electron reduction of C_{60} in colloidal TiO_2 semiconductor suspensions. J Phys Chem 98:9137-9142

31. Briggs D, Beamson G (1992) The Scienta ESCA300 Data base, John Wiley & Sons Inc, New York, p 266

32. http://srdata.nist.gov/xps/Default.aspx

33. Gamero M, Sosna M, Pariente F, Lorenzo E, Bartlett PN, Alonso C (2012) Influence of macroporous gold support and its functionalization on lactate oxidase-based biosensors response. Talanta 94:328-334

34. Wang K, Xu JJ, Chen HY (2006) Biocomposite of cobalt phthalocyanine and lactate oxidase for lactate biosensing with MnO_2 nanoparticles as an eliminator of ascorbic acid interference. Sens Actuators B 114:1052–1058

35. Parra AM, Casero E, Vázquez L, Pariente F, Lorenzo E (2006) Design and characterization of a lactate biosensor based on immobilized lactate oxidase onto gold surfaces. Analytica Chimica Acta 555:308–315.

FIGURE CAPTIONS

Figure S1. (A) XRD pattern, (B) AFM image of TiO_2-NPs deposited onto a Si/SiO_2 substrate, (C) Height distribution corresponding to the image in figure S1B.

Figure S2. 10 mM TiO_2 colloidal suspension in ethanol (A), mixture of GO and TiO_2 colloidal suspension before (B) and after (C) 3 hours of UV irradiation. (D) Mechanism of the TiO_2-UV-assisted photocatalytic reduction of graphene oxide.

Figure 1. (A) 1.6 x 1.6 μm^2 AFM image of a photocatalytically reduced graphene sheet with TiO_2 nanoparticles on Si/SiO_2 substrate obtained in dynamic mode at air. (B) Height distribution corresponding to the image in figure 1A. The height difference between the two maxima corresponds to the average thickness of the platelet structure.

Figure 2. . Raman spectra of GO and TiO_2/PRG samples. Red and blue lines are the fits of the experimental data for GO and TiO_2/PRG respectively. Excitation at 488 nm.

Figure 3. C1s XPS spectra of (A) graphene oxide (GO) and (B) photocatalytically reduced graphene (TiO_2/PRG). The decomposition in curve components is shown in color scale underneath the data points. The black line corresponds to the sum of all the individual components.

Figure 4. (A) Cyclic voltammetric response in 0.1 M phosphate buffer pH=7 containing 1.0 mM HMF for: a) LOx/GC in the absence of lactate, b) LOx/GC in the presence of 3 mM of lactate and c) LOx/TiO_2/PRG/GC in the presence of 3 mM of lactate. Scan rate 0.01 V/s. (B) Calibration curve obtained from chronoamperometric measurements (E=+0.25 V) for LOx/TiO_2/PRG/GC biosensor in phosphate buffer 0.1 M pH=7

containing 1.0 mM HMF in presence of increasing amounts of lactate. Inset: Linear part of 5B and the corresponding fit to a linear regression equation.

Table 1. Analytical properties of several lactate based biosensors reported in the literature including the present work.